The Astrophysical Journal, 908:57 (8pp), 2021 February 10 https://doi.org/10.3847/1538-4357/abd93c

Observational Support for Massive Black Hole Formation Driven by Runaway Stellar Collisions in Galactic Nuclei

Andrés Escala
Departamento de Astronomía, Universidad de Chile, Casilla 36-D, Santiago, Chile; aescala@das.uchile.cl
Received 2020 August 31; revised 2020 December 29; accepted 2021 January 1; published 2021 February 11

Abstract

We explore a scenario for massive black hole formation driven by stellar collisions in galactic nuclei, proposing a new formation regime of global instability in nuclear stellar clusters triggered by runaway stellar collisions. Using order-of-magnitude estimations, we show that observed nuclear stellar clusters avoid the regime where stellar collisions are dynamically relevant over the whole system, while resolved detections of massive black holes are well into such collision-dominated regimes. We interpret this result in terms of massive black holes and nuclear stellar clusters being different evolutionary paths of a common formation mechanism, unified under the standard terminology of both being central massive objects. We propose a formation scenario where central massive objects more massive than $\sim 10^8\,M_\odot$, which also have relaxation times longer that their collision times, will be too dense (in virial equilibrium) to be globally stable against stellar collisions, and most of the mass will collapse toward the formation of a massive black hole. Contrarily, this will only be the case at the core of less dense central massive objects, leading to the formation of black holes with much lower black hole efficiencies $\epsilon_{\rm BH} = \frac{M_{\rm BH}}{M_{\rm CMO}}$, with these efficiencies $\epsilon_{\rm BH}$ drastically growing for central massive objects more massive than $\sim 10^7\,M_\odot$, approaching unity around $M_{\rm CMO} \sim 10^8\,M_\odot$. We show that the proposed scenario successfully explains the relative trends observed in the masses, efficiencies, and scaling relations between massive black holes and nuclear stellar clusters.

Unified Astronomy Thesaurus concepts: Supermassive black holes (1663); Star clusters (1567); Relaxation time (1394); Collision processes (2065); Scaling relations (2031)

1. Introduction

For more than half a century, evidence was accumulated for the existence of massive black holes (MBHs) in galactic nuclei with masses of $\sim 10^{6-9}\,M_\odot$ (Zel'dovich 1964; Salpeter 1964; Ghez et al. 2008; Gillessen et al. 2009), but only recently did definite support arrive in favor of their existence (The Event Horizon Telescope Collaboration 2019). The origin of such "monsters" puzzled theorists soon after their discovery (Rees 1984); however, their dominant formation process is still a mystery (Volonteri 2010). With the advent of gravitational-wave astronomy, especially with the future LISA experiment (Amaro-Seoane et al. 2013; Barause et al. 2015), it is expected to that we will have definite answers on the formation of MBHs in the universe.

Several pathways have been proposed for MBH formation (Rees 1984; Shapiro 2004; Volonteri 2010), which can be briefly summarized in three channels: (i) direct collapse of a primordial cloud onto an MBH (Bromm & Loeb 2003; Lodato & Natarajan 2006; Latif & Schleicher 2015; Becerra et al. 2015; Regan & Downes 2018), (ii) growth by gas accretion and/or mergers of a stellar/intermediate-mass BH up to the mass range of MBHs (Madau & Rees 2001; Volonteri et al. 2003; Agarwal et al. 2013; Ricarte & Natarajan 2018), and (iii) formation of an MBH by catastrophic stellar collisions in dense stellar clusters (Zel'dovich & Podurets 1965; Rees 1984; Shapiro & Teukolsky 1985, Omukai et al. 2008; Devecchi & Volonteri 2009; Devecchi et al. 2012). However, all of them faced severe problems in fulfilling the constraints set by observations, such as the physical conditions needed to sustain atomic cooling halos are unclear to be fulfilled in nature (item (i); Shang et al. 2010; Inayoshi & Haiman 2014; Suazo et al. 2019), problems explaining the highest-redshift quasars with lower-mass BHs grown through Eddington-limited accretion (item (ii); Gnedin 2001; Volonteri & Rees 2006; Prieto et al. 2017; Inayoshi et al. 2020), and that simulations of stellar collisions in dense clusters are able to form only BHs of lower masses in the intermediate-mass regime (item (iii); Portegies Zwart & McMillan 2002; Freitag et al. 2006a, 2006b; Goswami et al. 2012; Stone et al. 2017).

Besides the problems faced by the different formation scenarios, galactic centers are arguably the most favorable places for MBH formation. Any gaseous (and stellar) material that eventually loses its orbital support falls onto this preferential place (Shlosman et al. 1990; Escala 2006), which corresponds to the deepest part of the galactic gravitational potential. Multiple processes produce strong inflows at galactic scales on dynamical timescales, funneling large amounts of gaseous material (up to $10^{10}\,M_\odot$) to this preferential place, including gravitational torques in galaxy mergers (Barnes 2002; Mayer et al. 2010; Prieto et al. 2020), bars within bars (Regan & Teuben 2004; Hopkins & Quataert 2010), clump migration by dynamical friction (Escala 2007; Elmegreen et al. 2008), etc. These processes are expected to be even more dramatic in the case of protogalactic material at high z because of the higher gas fractions and absence of AGN feedback from preexisting MBHs (Prieto & Escala 2016). Therefore, in the absence of feedback limiting factors (Dubois et al. 2015; Prieto et al. 2017), the amount of material funneled into galactic nuclei has (in principle) no upper limit externally set by processes at galactic scales; thus, we expect to be the hosting place of the densest gaseous and stellar configurations in the universe. The straightforward question is then, if such material does not end up forming an MBH that corresponds to gravity's final triumph, which other stable physical configuration (at intermediate densities) could it be?

The hypothetical scenario under very efficient heating mechanisms ($T_{\rm vir} \geqslant 10^4$ K) has been extensively studied (Bromm & Loeb 2003; Lodato & Natarajan 2006; Latif & Schleicher 2015; Becerra et al. 2015; Regan & Downes 2018), where fragmentation is suppressed on smaller scales and that leads directly to the formation of a single very massive quasi-star (VMS; Volonteri & Begelman 2010; Schleicher et al. 2013) at the center, which afterward collapses onto an MBH due to post-Newtonian instability (Tolman 1934; Oppenheimer & Volkoff 1939). Contrarily, in the absence of efficient heating, the gaseous material funneled to the galactic center efficiently cools (Rees & Ostriker 1977; Sarazin & White 1987), eventually becomes unstable, and fragments in a broad range of scales (Toomre 1964; Escala & Larson 2008; Escala 2011), leading to the formation of a dense stellar cluster (Bate et al. 2003; Padoan et al. 2016). Such dense stellar configurations, called nuclear stellar clusters (NSCs), are indeed observed and considered to be the densest stellar configurations in the local universe (Böker et al. 2004; Côté et al. 2006; Walcher et al. 2006; Balcells et al. 2007), located in galactic nuclei and in some cases coexisting with an MBH (Leigh et al. 2012; Georgiev et al. 2016) and thus possibly being a joint formation event. Therefore, a more realistic scenario reduces to how dense such a stellar system it can be before becoming globally unstable, again leading to the formation of an MBH.

A natural candidate for triggering instability in stellar clusters are collisions between stars since it is an efficient mechanism for loosing orbital energy support, because physical collisions between stars are a dissipative source on a fluid interpretation of a cluster, being able to convert energy in kinetic motions into internal heat of stars and that otherwise, without collisions the energy in stellar motions behaves adiabatically. However, it is generally believed that physical collisions between stars are considered an exotic phenomenon that rarely happens in the universe (Binney & Tremaine 2008), restricted to only being relevant in the cores of dense stellar configurations like globular cluster systems (Portegies Zwart et al. 1999), where it is well established that the cores of such dense stellar systems are unstable to suffer catastrophic runaway stellar collisions (Portegies Zwart & McMillan 2002). Numerical experiments have shown that runaway collisions of the most massive stars could led to the formation of intermediate-mass BHs (IMBHs) in the centers of typical globular clusters (BH masses $\sim 10^3\ M_\odot$ can be built up before the first supernova explodes; Portegies Zwart & McMillan 2002; Gurkan et al. 2004; Freitag et al. 2006a, 2006b). Nevertheless, it is unclear what could happen in the more extreme conditions of the protogalactic nucleus because of the lack of detailed N-body simulations that include the effects of the higher densities and velocity dispersions, which, in addition to gas dissipation, should define a density limit for NSCs before becoming globally unstable to catastrophic stellar collisions.

In this paper, we will study the role of runaway stellar collisions in galactic nuclei, particularly in the global stability of NSCs and the possible formation of MBHs. We start quantifying the role of collisions in NSCs in Section 2. We continue in Section 3, proposing a scenario for MBH formation in galactic nuclei from NSCs. Finally, we discuss the results of the proposed scenario and its implications for the high-redshift universe in Section 4.

2. Quantifying the Role of Collisions in NSCs

An order-of-magnitude estimate that quantifies the occurrence of collisions in any system with a large number of particles is to compute a collision timescale given by $t_{\rm coll} = \lambda/\sigma$, where σ is the characteristic (dispersion) velocity of the system and λ is the particle (star) mean free path (Binney & Tremaine 2008). From the equation $n\Sigma_o\lambda = 1$, a mean free path can be probabilistically defined (Landau & Lifshitz 1980; Shu 1991), where n is the number density of stars and Σ_o is the effective cross section, giving a collision rate of $t_{\rm coll}^{-1} = n\Sigma_o\sigma$. This is a widely used definition for collision timescale, accurate enough for the general purposes of this paper; for a more specific formula that could be better for quantifying collision rates in a particular problem, see, for example, Leigh et al. (2014). Assuming that the stellar system is virialized, the dispersion velocity is $\sigma = (GM/R)^{1/2}$, where M is the total mass and R is the characteristic radius of the system. This result is generally valid in any stellar system in virial equilibrium, as well as for systems with a relevant dark matter component, using the empirically calibrated formula of Cappellari et al. (2006), where the velocity dispersion is $\sigma = (GM/5f_gR)^{1/2} \approx (GM/R)^{1/2}$ for $f_g = 0.16$ (Spergel et al. 2003). Therefore, in any virialized stellar system, the collision timescale is given by

$$t_{\rm coll} = \frac{1}{n\Sigma_o}\sqrt{\frac{R}{GM}}. \tag{1}$$

In a uniform system, composed only of equal-mass stars with masses $\eta\, M_\odot$, the number density is $n = 3M/4\pi R^3 \eta\, M_\odot$. The effective cross section Σ_o, due to gravitational focusing, is for a solar-mass star of approximately $100\,\pi R_\odot^2$ (i.e., Equation (7.195) in Binney & Tremaine 2008, with a Safronov number for solar-mass stars with $\sigma \sim 100\,{\rm km\,s^{-1}}$; Leigh et al. 2012). Under these assumptions, neglecting radial concentrations, initial mass functions, and other dimensionless factors of order unity, collisions will be relevant in the dynamics (and possibly becoming unstable) of a given system with a characteristic age $t_{\rm H}$, if its age is comparable or longer than the collision time, $t_{\rm coll} \leqslant t_{\rm H}$, which is equivalent to the following condition:

$$\hat{\rho}_{\rm crit} \equiv \left(\frac{4\eta\, M_\odot}{300 R_\odot^2 t_{\rm HG}^{1/2}}\right)^{2/3} \leqslant {\rm MR}^{-\frac{7}{3}}, \tag{2}$$

where $\hat{\rho}_{\rm crit}$ is a critical mass density, an intermediate density between the surface density ($\propto R^{-2}$) and a volumetric one ($\propto R^{-3}$). The largest relevant value for $t_{\rm H}$ is the age of the universe, which is of the order of $\sim 10^{10}$ yr (Spergel et al. 2003), that gives (for solar-mass stars, $\eta = 1$) a minimal critical mass density $\hat{\rho}_{\rm crit} \sim 10^7\, M_\odot {\rm pc}^{-7/3}$, but galactic centers can be 1 order of magnitude younger ($t_{\rm H} \sim 10^9$ yr). Within geometrical factors of order unity, such a boundary is set by a combination of a fundamental constant (G), with typical parameters of our universe such as its current age ($t_{\rm H}$) and the properties of the Sun ($M_\odot$, $R_\odot$), which it is considered to be an average star in the universe and thus making $\eta = 1$ the most obvious choice, defining the critical density of stable stellar systems for our current cosmic parameters. Also, we arrive at such a criterion without ad hoc assumptions, being the only assumption to be virialized, which is only a requirement for being a stationary stellar system.

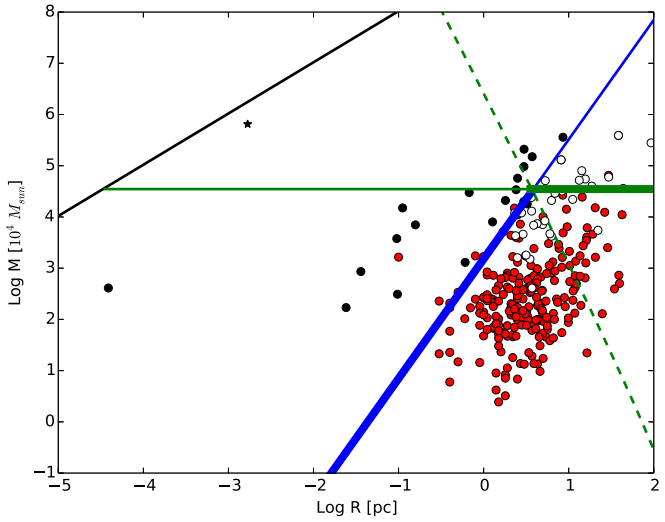

Figure 1. Measured masses and effective radii for NSCs (red circles), "well-resolved" MBHs (black circles), and "unresolved" MBHs (white circles). The measurement of M87's BH shadow (The Event Horizon Telescope Collaboration 2019) is denoted by the black star, which is the closest to the black line that represents positions of the Schwarzschild radius as a function of mass. The solid blue line represents the condition given by Equation (2) for $t_{\rm H} = 10^{10}$ yr ($\hat{\rho}_{\rm crit} \sim 10^7\,M_\odot$ pc$^{-7/3}$ for solar-mass stars, $\eta = 1$). The horizontal green line represents the condition implied by Equation (3) ($\sim 3.5 \times 10^8\,M_\odot$) in order to be in agreement with the observed scaling relation for NSCs (Leigh et al. 2012). The dashed green line denotes the condition given by Equation (4) for $t_{\rm H} = 10^{10}$ yr, which intersects the solid blue line at the same critical mass determined by the condition given by Equation (3). The positions of NSCs are restricted within the boundaries defined by the collisional stable region for NSCs, denoted by the thicker blue and green lines.

Figure 1 displays the observed masses and effective radii for NSCs in both late- and early-type galaxies (red circles) taken from Georgiev et al. (2016). The solid blue line in Figure 1 displays the condition given by Equation (2) for $t_{\rm H} = 10^{10}$ yr and $\eta = 1$ (solar-mass stars). The measured properties of NSCs (red circles) show a clear avoidance of the regions in which collisions could be globally relevant in the internal dynamics of a cluster, with collision timescales always larger than the age of the universe (right side of the solid blue line). The only clear exception is NGC 1507, with its $\geqslant 10^7\,M_\odot$ in only 0.1 pc of effective radius; however, this last measurement has estimated errors over 2000% (an effective radius up to 2.3 pc that moves NGC 1507 to the right side of the blue line). It is important to note that these are average collision timescales, relevant for global stability against collisions, and that they can be considerably shorter at the core; therefore, these globally stable NSCs can still coexist with an unstable core, which is expected to be triggered by Spitzer's instability (Spitzer 1969; Vishniac 1978; Portegies Zwart & McMillan 2002).

In addition, we plot in Figure 1 the measured masses and resolution radius ($=0.5 d_{\rm resol}$, where $d_{\rm resol}$ is the observation spatial resolution) for MBH candidates, but we differentiate them between "well-resolved" MBHs with an influence radius $R_{\rm inf}$ larger than three spatial resolutions (black circles) and "unresolved" ones ($R_{\rm inf} < 3\,d_{\rm resol}$) with white circles, both from the sample of Gultekin et al. (2009). Contrary to the case of nuclear clusters, in the case of MBH candidates, we see two clear trends: the properties of resolved MBHs are in the region that clearly passed to the collision-dominated regime (left side of the solid blue line), and the unresolved ones still avoid the collision-dominated regime and coexist with the NSCs.

The trend for unresolved MBH positions can be easily understood by taking into account that the properties of MBHs are diluted due to resolution. For the unresolved MBHs, this means a decrease in densities down to values comparable to stellar densities in the nuclear regions of their host. Therefore, the unresolved MBHs can be taken as better estimates of the properties of the stellar background within $R_{\rm inf}$ than of MBHs themselves, and in some sense, they can be considered like stellar systems. Taking this into account, the properties of NSCs clearly differ from those of resolved MBHs, with NSCs avoiding the collision-dominated region and resolved MBHs passing such a limit, with a sharp transition from NSCs to resolved MBHs around $t_{\rm coll}$ of the order of the age of the universe.

Taking also into account that for a virialized system, $R = GM/\sigma^2$, the condition given by Equation (2) can be rewritten as

$$\sqrt{\frac{4\,\eta\,R_\odot}{300\,\sigma_\odot t_H}} \leqslant \frac{M_\odot}{M}\left(\frac{\sigma}{\sigma_\odot}\right)^{3.5}, \qquad (3)$$

with $\sigma_\odot = \sqrt{\frac{G\,M_\odot}{R_\odot}} \sim 400$ km s^{-1}. If this condition is combined with the empirical scaling relation that constrains the properties for observed NSCs, $\frac{M_{\rm NSC}}{10^{6.9} M_\odot} = \left(\frac{\sigma}{128\ {\rm km\ s^{-1}}}\right)^{2.73} \sim \left(\frac{3\sigma}{\sigma_\odot}\right)^{2.73}$ (Leigh et al. 2012), it shows that NSCs will be unstable for masses larger than $\sim 3.5 \times 10^8\,M_\odot$ (for a $t_{\rm H}$ again of the order of the age of the universe and for solar-mass stars, $\eta = 1$). This condition is denoted by the horizontal green line in Figure 1, again showing good agreement with the value of the most massive NSCs. Therefore, besides these conditions being order-of-magnitude estimations with simplifications, the positions of NSCs are suggestively restricted within the boundaries defined by the collisional stable region, denoted by the thicker blue and green lines in Figure 1.

Although this trend of NSCs in Figure 1 is very suggestive, its interpretation is nevertheless more complicated, since several additional factors need to be taken into account. In addition to the intrinsic idealizations of these order-of-magnitude estimations, one very relevant factor is that Figure 1 compares the structural properties of NSCs currently observed, not at the time of formation, which can be smaller by a factor of 10 or more in radius (Banerjee & Kroupa 2017); therefore, evolutionary processes must be taken into account. Numerical studies of the long-term evolution of NSCs (and with MBHs; Baumgardt et al. 2018; Pamanarev et al. 2019) have shown that their effective radius indeed expands, which implies that NSCs moved from left to right in Figure 1 as they evolved. Such expansion is expected to happen in a self-similar manner when it is only due to two-body relaxation processes ($R \propto t^{2/3}$; Henon 1965; Gieles et al. 2012).

The two-body relaxation time is the relevant timescale for this evolution expected in the position of NSCs in Figure 1, because it quantifies the energy exchange by two-body scattering and is generally expressed as $t_{\rm relax} \approx \frac{0.1N}{lnN}\,t_{\rm cross}$ (Binney & Tremaine 2008), where $t_{\rm cross}$ is the crossing time of the cluster and N is its total number of stars. For a virialized system, the crossing time is given by $t_{\rm cross} = R/\sigma = R^{3/2}/\sqrt{GM}$, and if it is composed of equal-mass stars, the total number of stars is simply $N = M/\eta M_\odot$. Under these assumptions, two-body relaxation will be relevant

in the evolution of a system with a characteristic age $t_{\rm H}$, if $t_{\rm H}$ is comparable to or longer than the relaxation time, $t_{\rm relax} \leqslant t_{\rm H}$, which is equivalent to the following condition:

$$R \leqslant \left(\frac{t_{\rm H}\eta\, M_\odot}{0.1}\ln\left(\frac{M}{\eta\, M_\odot}\right)\right)^{2/3}\left(\frac{G}{M}\right)^{1/3}. \quad (4)$$

The dashed green line in Figure 1 denotes the condition given by Equation (4) for a characteristic cluster age comparable to the age of the universe ($t_{\rm H} = 10^{10}$ yr) and composed of solar-mass stars ($\eta = 1$), showing an intersection with the solid blue line strikingly at the same critical mass determined by the condition given by Equation (3). An NSC that has $t_{\rm relax} \leqslant t_{\rm coll}$ (with cluster mass below the intersection) could start with a collision time shorter than the age of the universe, but its effective radius will expand before collisions become important, moving its position to the collisional stable region (right side of the solid blue line). On the other hand, if $t_{\rm coll} \leqslant t_{\rm relax}$, the NSCs will not be able to expand before the onset of collisions, thus possibly becoming globally unstable against collisions. Therefore, this condition naturally explains the absence of NSCs for masses larger than the intersection of the dashed green and solid blue lines ($M_{\rm NSC} \gtrsim 4\times10^8\, M_\odot$). It is important to emphasize that this stability condition comes from the triple equality: $t_{\rm relax} = t_{\rm coll} = t_{\rm H}(\sim 10^{10}$ yr).

Moreover, since the NSCs are clustered below the intersection of blue and dashed green lines in Figure 1 ($t_{\rm relax} \leqslant t_{\rm coll}$), their collision times measured today can be assumed to be longer than at the formation of the NSCs, before their (effective) radius increased. Therefore, the NSCs that today display a collision time slightly longer than the age of the universe could have had a considerably shorter collision time at formation, suggesting that those NSCs at formation crossed the condition of being in the collision-dominated regime, $t_{\rm coll} \leqslant t_{\rm H}$, but were reversed since $t_{\rm relax} \leqslant t_{\rm coll}$, meaning that the initial conditions of galactic nuclei can indeed fulfill the conditions for instability, at least temporarily, and that many NSCs were at the edge of collisional instability at formation. Under different circumstances are resolved MBHs, all in the collisional-dominated regime in Figure 1 ($t_{\rm coll} \leqslant t_H$), independent to the relative value of $t_{\rm relax}$, suggesting two different channels for MBH formation at least. This fact motivates us to explore a joint MBH–NSC formation scenario in the next section in order to explain their relative trends in Figure 1.

3. A Scenario for MBH Formation in Galactic Nuclei from Nuclear Star Clusters

Both MBHs and NSCs are observed to coexist in the nuclei of galaxies (Leigh et al. 2012; Georgiev et al. 2016) suggesting to be a generic byproduct of their formation and evolution, being two completely distinct type of objects unified into the terminology of being a central massive object (CMO; Ferrarese et al. 2006). The MBHs dominate in galaxies with masses larger than $10^{12}\, M_\odot$ and similarly occur with NSCs for galaxies less massive than $10^{10}\, M_\odot$, with both coexisting in the intermediate-mass regime (Georgiev et al. 2016). If they are indeed different evolutionary stages of a common formation mechanism, the simplest interpretation of their different locations in Figure 1 is in terms of MBHs and NSCs being CMOs with different final fates. The CMOs that are too dense to be globally stable against stellar collisions and that also fulfill the condition $t_{\rm coll} \leqslant t_{\rm relax}$, thus being unable to expand before the onset of runaway collisions, will probably collapse toward the formation of an MBH. Contrarily, this will only be the case at best in the core of less dense clusters, being globally stable in the form of an NSC, probably coexisting in its center with a lower-mass BH formed in the unstable core.

Numerical simulations of globular-type stellar clusters ($\leqslant 10^6\, M_\odot$) show that cores are unstable to suffer catastrophic runaway stellar collisions of massive stars due to Spitzer's instability (Portegies Zwart & McMillan 2002), as long as the cluster is enough massive and concentrated, with core-collapse (relaxation) times less than those set by the evolution of their massive stars (<3–25 Myr). A central most massive object is generically formed with efficiencies ranging from 0.1% (Portegies Zwart & McMillan 2002; Freitag et al. 2006a, 2006b) up to a few percent of the cluster mass (Sakurai et al. 2018; Reinoso et al. 2018), depending on multiple physical parameters such as stellar radius, (initial) stellar mass distribution, etc. The central most massive object is expected to a have similar fate as a VMS, typically being out of thermal equilibrium with a Kelvin–Helmholtz timescale larger than the collision timescale (Goswami el al. 2012), and is also expected to collapse to an IMBH due to post-Newtonian instability (Tolman 1934; Oppenheimer & Volkoff 1939).

Unfortunately, direct N-body simulations do not explore either the regime of larger clusters in the NSC mass range ($>10^6\, M_\odot$) or the more extreme regime of globally unstable clusters ($>10^8\, M_\odot$), not only because its properties are more exotic but also because they are numerically much more expensive. The few exceptions are restricted to either Monte Carlo calculations (Sanders 1970; Gurkan et al. 2004) or self-consistent Fokker–Planck models of galactic nuclei (Lee 1987; Quinlan & Shapiro 1990), but their results are already quite suggestive, finding that in large N systems ($>10^7$ stars, which corresponds to cluster masses larger than $10^7\, M_\odot$, assuming solar-mass stars), three-body binary heating is unable to reverse core collapse before the onset of runaway collisions and then is vulnerable to a "merger instability," which may lead to the formation of a central BH (Lee 1987; Quinlan & Shapiro 1990). Since in this regime, the collision runaway started well before core collapse and for a system with (initially) equal-mass stars (Lee 1987; Quinlan & Shapiro 1990), without even requiring Spitzer's instability, it is reasonable to expect in those system efficiencies $M_{\rm BH}/M_{\rm cluster}$ higher than the few percent found in N-body simulations of globular-type stellar clusters. The NSCs are indeed expected to be the most favorable places for stellar collisions in the universe.

More recently, Davies et al. (2011) and Miller & Davies (2012) extended the work of Quinlan & Shapiro (1990) using analytical estimations to determine the stability of NSCs against stellar collisions. In particular, Miller & Davies (2012) studied different paths for MBH formation in NSCs and determined that MBHs should form in NSCs with velocity dispersions $\gtrsim$40 km s^{-1}, since primordial binaries might not provide enough heat via single-binary interactions that could support core collapse as in Lee (1987) and Quinlan & Shapiro (1990). They found that during or after full core collapse, the stars will undergo runaway collisions that produce a BH, which will then grow via tidal disruption of stars, a process that is expected to scale as $M_{\rm BH}(t) \sim 10^6 M_\odot(\sigma/50\ {\rm km\ s^{-1}})^{3/2}\sqrt{t/10^{10}\ yr}$ (Stone et al. 2017). This can be considered further evidence to expect in galactic nuclei $M_{\rm BH}/M_{\rm cluster}$ efficiencies higher than the few

percent found in *N*-body simulations of globular-type stellar clusters.

Nevertheless, for velocity dispersions $\gtrsim 100\,\mathrm{km\,s^{-1}}$, Miller & Davies (2012) argued an NSC will typically have too long a relaxation time for its core to collapse within a Hubble time, a condition equivalent to the right side of the dashed green line in Figure 1. However, they missed the possible new regime of global instability proposed here for $t_{\rm coll}(\leqslant t_{\rm H}) \leqslant t_{\rm relax}$ for masses larger than when the dashed green line in Figure 1 intersects the solid blue line, and that strikingly coincides with the maximum mass scale with the presence of NSCs in galactic nuclei. For $t_{\rm coll} \leqslant t_{\rm relax}$, relaxation processes will be unable to reverse global collapse before the onset of runaway collisions, which may lead to global collapse onto the formation of an MBH. Since the condition $t_{\rm coll} \leqslant t_{\rm relax}$ in Figure 1 is computed for total NSC quantities, it is valid over the whole system and not restricted to the core and also valid independent of different processes favoring or quenching core collapse analyzed by Miller & Davies (2012).

Therefore, Figure 1 is supporting evidence that, in addition to NSCs being the most favorable places for stellar collisions, the most massive and denser NSCs that form in the universe might exist only temporarily, being, in principle, globally unstable to collapse to an MBH. This instability should eventually be triggered by runaway stellar collisions at some density limit, regardless of whether it is at the $\hat{\rho}_{\rm crit}$ defined by Equation (2) (for $t_{\rm coll} \leqslant t_{\rm relax}$) or another criterion that includes processes such as gas dissipation and others not taken into account. It is then possible to visualize the following transition in the properties of CMOs: for objects denser than some critical limit—which, from the intersection defined by Equations (2) and (4) at $t_{\rm H} \sim 10^{10}$ yr or Equation (3) in order to fulfill the observed scaling relation for NSCs (Leigh et al. 2012), seems to be the case for $M_{\rm CMO} \gtrsim 4 \times 10^8\,M_\odot$—most of the CMO mass will be in the form of an MBH. On the opposite mass limit, the bulk of mass in the CMO will stay in the stars of the NSC, even in some cases with an undetectable MBH at its center, with BH efficiencies $\epsilon_{\rm BH} = M_{\rm BH}/M_{\rm CMO}$ probably in the range of star cluster simulations from 0.1% up to a few percent (Portegies Zwart & McMillan 2002; Freitag et al. 2006a, 2006b; Sakurai et al. 2018; Reinoso et al. 2018) until it approaches a second critical mass ($M_{\rm CMO} \sim 10^7\,M_\odot$; according to Lee 1987; Quinlan & Shapiro 1990; Miller & Davies 2012; Stone et al. 2017), where the BH efficiency should have a drastic change, rapidly growing toward $\epsilon_{\rm BH}$ close to 1.

3.1. Testing the Scenario for MBH Formation and Implications for Scaling Relations

The concordance of the proposed scenario for CMO evolutionary paths with the observed relative masses in MBHs and NSCs can be easily tested. Assuming that is the total mass in CMOs, the mass reservoir for which MBHs and NSCs compete in the galactic nucleus, $M_{\rm CMO} = M_{\rm NSC} + M_{\rm BH}$, for a BH formation efficiency ($\epsilon_{\rm BH}$), the central BH mass is $M_{\rm BH} = \epsilon_{\rm BH}\,M_{\rm CMO}$, and the mass of the surrounding nuclear cluster is then $M_{\rm NSC} = (1-\epsilon_{\rm BH})\,M_{\rm CMO}$, both related to the efficiency as $\epsilon_{\rm BH} = \left(1 + \frac{M_{\rm NSC}}{M_{\rm BH}}\right)^{-1}$, which then can be directly estimated by measuring the masses $M_{\rm NSC}$ and $M_{\rm BH}$. Also, assuming that is total mass in CMOs $M_{\rm CMO}$ the one that correlates with the total mass of the host spheroid

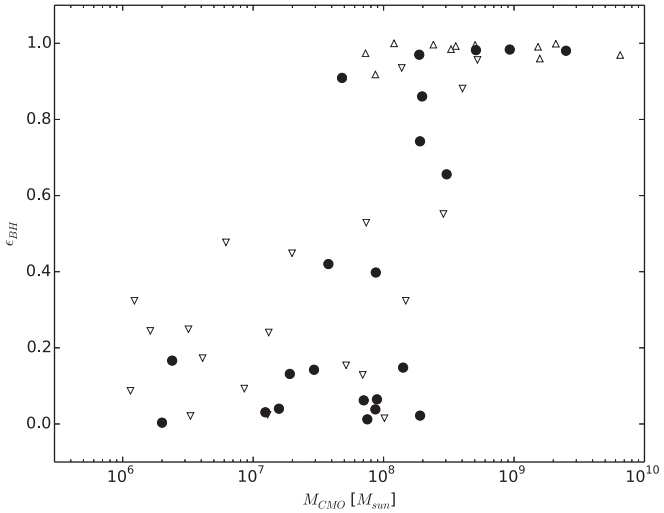

Figure 2. Observed BH formation efficiency $\epsilon_{\rm BH} = \left(1 + \frac{M_{\rm NSC}}{M_{\rm BH}}\right)^{-1}$ as a function of the total mass in CMOs, $M_{\rm CMO} = M_{\rm NSC} + M_{\rm BH}$, with both quantities computed using the MBH and NSC masses from the data set by Neumayer et al. (2020), represented by black circles. The efficiency displayed in the figure has two dominant values for BH efficiencies ($\epsilon_{\rm BH} \leqslant 0.15$ at $M_{\rm CMO} \leqslant 3 \cdot 10^7\,M_\odot$ and $\epsilon_{\rm BH} \geqslant 0.9$ for $M_{\rm CMO} \geqslant 3 \cdot 10^8\,M_\odot$) and a transition close to a step function of the mass. Upper limits for the efficiencies $\epsilon_{\rm BH}$ are denoted by downward-pointing triangles, while lower limits for $\epsilon_{\rm BH}$ are denoted by upward-pointing triangles, displaying the same trend as the black circles but with larger scatter at lower CMO masses.

($M_{\rm CMO} = \epsilon M_{\rm sph}$, with $\epsilon \sim 0.1\%$; Magorrian et al. 1998), it is straightforward to realize that in both limiting cases (either only an MBH or NSC), the observed (individual) relations are automatically fulfilled ($M_{\rm NSC} \sim \epsilon M_{\rm sph}$ for $\epsilon_{\rm BH} \sim 0$ and $M_{\rm BH} \sim \epsilon M_{\rm sph}$ for $\epsilon_{\rm BH} \sim 1$).

Figure 2 displays the efficiencies $\epsilon_{\rm BH} = \left(1 + \frac{M_{\rm NSC}}{M_{\rm BH}}\right)^{-1}$ plotted against the total mass in CMOs ($M_{\rm CMO} = M_{\rm NSC} + M_{\rm BH}$), with both quantities computed using measured masses from a data set recently collected (and homogenized) in the review by Neumayer et al. (2020), denoted by black circles in the figure. The data in Figure 2 clearly display three regimes: (a) $\epsilon_{\rm BH} \leqslant 0.15$ for $M_{\rm CMO} \leqslant 3 \cdot 10^7\,M_\odot$, (b) $\epsilon_{\rm BH} \geqslant 0.9$ for $M_{\rm CMO} \geqslant 3 \cdot 10^8\,M_\odot$, and (c) a transition regime in the range $3 \cdot 10^7\,M_\odot \leqslant M_{\rm CMO} \leqslant 3 \cdot 10^8\,M_\odot$ with rapidly growing $\epsilon_{\rm BH}$. Upper limits for the efficiencies $\epsilon_{\rm BH}$ are denoted by downward-pointing triangles, while lower limits for $\epsilon_{\rm BH}$ are denoted by upward-pointing triangles, displaying the same trend as the black circles but with a larger scatter, as expected for upper and lower limits. This trend is clear and suggestively in agreement with the proposed formation scenario for CMOs, with the transition regime limited on the expected boundaries defined by the "merger instability" found in Fokker–Planck models of galactic nuclei ($\gtrsim 10^7\,M_\odot$; Lee 1987; Quinlan & Shapiro 1990) and the upper limit given by the condition $t_{\rm coll} \leqslant t_{\rm relax}$ ($\gtrsim 10^8\,M_\odot$, also in agreement with Equation 3 to fulfill the scaling relation for NSCs; Leigh et al. 2012). This can be contrasted, for example, with BH efficiencies $\epsilon_{\rm BH}$ that are randomly distributed between zero and 1, which could be the case in a different formation scenario, where most (75%) of the measurements should be in the interval $\epsilon_{\rm BH} = [0.15,\ 0.9]$ and there is a total absence of black circles in regimes (a) and (b) of Figure 2. Moreover, a sharp transition is also seen around $M_{\rm CMO} \sim 10^8\,M_\odot$, suggesting again that this is the limit for

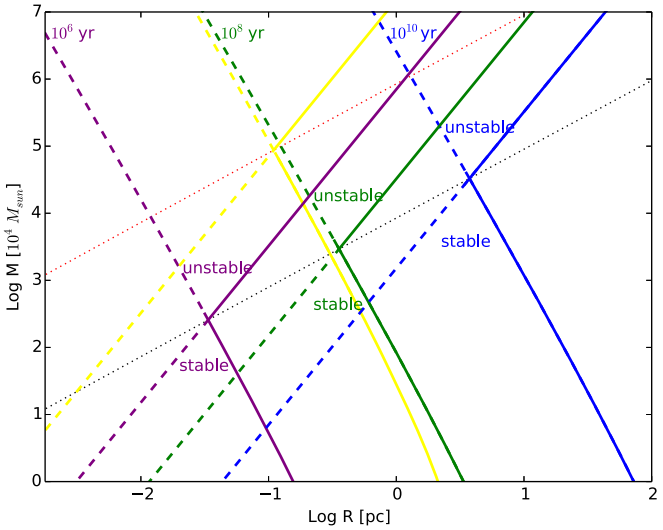

Figure 3. Collision and relaxation timescales in the mass vs. radius diagram for clusters composed of solar-mass stars ($\eta = 1$) for different cluster ages t_H: 10^{10} (blue), 10^8 (green), and 10^6 (purple) yr. For each color with a different t_H, clusters on the left side of the solid curves fulfill the condition $t_{coll} \leqslant t_H$ or $t_{relax} \leqslant t_H$, with the intersection of the solid curves dividing the stable ($t_{relax} \leqslant t_{coll}$) and unstable ($t_{coll} \leqslant t_{relax}$) regions. The yellow lines denote the same conditions for 100 $M_\odot$ Population III stars with $t_H = 10^6$ yr. The dotted black line denotes the condition $t_{relax} = t_{coll}$ for clusters composed of solar-mass stars ($\eta = 1$), and the dotted red line denotes clusters of more massive Population III stars ($\eta = 100$).

(collision-driven) global collapse, where most of the mass ends up in a single MBH and that naturally explains the lack of NSCs around MBHs for $M_{BH} \gtrsim 4 \cdot 10^8\, M_\odot$ (Georgiev et al. 2016).

The efficiency displayed in Figure 2, with two dominant values for BH efficiencies and a transition with a form close to a step function of the mass, could also explain the origin in the change of scaling in the M–σ relation from NSCs to MBHs, which has been taken as support that MBHs and NSCs may not share a common origin (Leigh et al. 2012). The empirical evidence is that NSCs have a less steep scaling relation, $M_{NSC} \propto \sigma^{2-3}$ (Leigh et al. 2012; Graham 2012), compared with the scaling for MBHs that have steeper slopes of $M_{BH} \propto \sigma^{4-5}$ (Ferrarese & Merritt 2000; Gebhardt et al. 2000). Assuming that CMOs have a single scaling relation originating in the galaxy formation process, for example, the scaling defined at the critical threshold given by Equation (3) ($M_{CMO} \propto \sigma^{3.5}$), the step function efficiency ϵ_{BH} shown in Figure 2 biases the relation for the less massive MBHs, giving a steeper slope (>3.5) for the MBH scaling relation and vice versa, with the $1 - \epsilon_{BH}$ bias, the original relation for the more massive NSC, giving a less steep slope (<3.5). Therefore, this naturally reconciles a scenario of joint formation, with different M–σ scaling relation for MBHs and NSCs.

It is important to note that alternative scenarios that are completely different from in situ NSC formation have also been explored to explain NSC properties and the different scaling relations for NSCs and MBHs. For example, a widely studied scenario is that NSCs form via merging of orbitally migrated globular clusters (Tremaine 1976; Capuzzo-Dolcetta 1993; Leigh et al. 2015). In those scenarios, tidal forces due to the gravity of an MBH can stop the NSC assembly by disrupting the orbitally infalling clusters, also leading to a maximum mass scale for NSCs in the presence of MBHs (Antonini et al. 2012; Arca-Sedda et al. 2015). Hybrid models of both migration of stellar clusters and in situ formation in galactic nuclei have also been explored by means of semianalytical/numerical models, which also explains the different M–σ relations for NSCs and SMBHs (Arca-Sedda & Capuzzo-Dolcetta 2014; Antonini et al. 2015). The biggest advantage of the scenario outlined in this paper is its simplicity, giving a clear cause for the sharp transition in Figure 2 for clusters becoming globally unstable against collisions for $t_{coll} \leqslant t_{relax}$, at the correct mass scale for clusters with ages comparable to the current age of the universe (Figure 1), that in addition naturally explains the different M–σ scaling relation for MBHs and NSCs, compared with the more complex (and multifactorial) explanations in these alternative models.

4. Discussion

We explored a scenario for MBH formation driven by stellar collisions in galactic nuclei, proposing a new formation regime of global instability in NSCs triggered by runaway stellar collisions for CMOs that have average relaxation times longer that their collision times. For systems with ages comparable to the Hubble time, this condition is fulfilled for objects more massive than $\sim 4 \times 10^8\, M_\odot$, being, in principle, subject to being globally unstable against stellar collisions, where most of its mass may collapse toward the formation of an MBH, being effectively the fate of the failed stellar cluster. Contrarily, this will only be the case at the core of less dense CMOs, leading to the formation of MBHs with much lower efficiencies ϵ_{BH}. We showed that the proposed scenario successfully explains the relative trends observed in the masses, efficiencies, and scaling relations between MBHs and NSCs.

The proposed scenario links naturally to the fact that the existence of MBHs in galaxies is intimately related to their spheroidal/triaxial component (Ferrarese & Merritt 2000; Gebhardt et al. 2000), which is supported by random motions and where collisions are much more frequent compared to the disk component of galaxies (for a given characteristic velocity), since disks are systems that are rotationally supported and their ordered motions prevent stellar collisions. In addition, this collision-driven global instability in extreme stellar systems internally sets the upper mass limit of NSCs around $\sim 10^8\, M_\odot$, something needed because, at galactic scales, the study of gravitational instabilities does not externally set an upper limit for the stellar cluster masses in galactic nuclei, since the size of the whole system is the largest unstable wavelength (Jeans 1902). Only when rotation becomes relevant (i.e., in the galactic disk) does this set a maximum mass scale for a gaseous collapsing cloud, ranging from $M_{cloud}^{max} \sim 10^6\, M_\odot$ for MW-type disks up to the order of $\sim 10^8\, M_\odot$ for ULIRG nuclear disks (Escala & Larson 2008). Those massive clouds in ULIRGs are expected to migrate and runaway merge in galactic nuclei (Elmegreen et al. 2008), again lacking an externally defined upper limit.

A relevant issue not studied extensively in this paper is the role of gas in the formation and evolution of NSCs, particularly the enhancement of stellar collisions. Although the details of the exact evolution of the gaseous (and stellar) material funneled into galactic nuclei are still unclear under realistic conditions, some idealized analytical estimations can be made. For example, Davies et al. (2011) concluded that a typical NSC at high z (mass $\sim 10^6\, M_\odot$ and size ~ 1 pc) can be contracted on dynamical timescales due to gas inflow with a mass up to 10

times heavier than the preexisting stellar mass (according to cosmological simulations; Bellovary et al. 2011), then reach a central density high enough for triggering a phase of runaway collisions that could form an MBH seed of $10^5\ M_\odot$ or larger. This scenario was simulated and numerically tested in a cosmological context by Lupi et al. (2014), who found it to be a feasible route that peaks at $z \lesssim 10$ and is competitive (in relative cosmological terms) with the formation of MBH seeds from the other, more traditional channels that were described in Section 1. Moreover, these high central densities (and thus runaway collisions) can be enhanced by the gaseous dynamical friction, which can be an efficient process to lead the migration of additional stellar compact remnants to galactic nuclei (Boco et al. 2020). Nevertheless, the presence of gas can also produce some temporal delays in the runaway growth of MBH seeds (Reinoso et al. 2018) by initially reducing the number of stellar collisions, but in the long term it compensates, the net effect being an increase of the final BH mass by a factor of 2 (Reinoso et al. 2018).

All of these gas dynamical processes relevant for high-z (proto)clusters act on fairly local dynamical timescales that are short compared to the current age of the universe; therefore, it is relevant to see how the proposed regime of collision-driven global instability can work under such shorter timescales. Figure 3 displays collision and relaxation timescales that are equal to cluster ages ($t_{\rm H}$) of 10^{10} (blue), 10^8 (green), and 10^6 (purple) yr, which illustrates that around 1 order of magnitude of contraction in effective radius (in a cluster of a given mass) —for example, due to the gaseous inflows expected at high z (Davies et al. 2011; Lupi et al. 2014)—can effectively reduce by almost 4 orders of magnitude the time required for collisions to become relevant (from $t_{\rm coll}$ being comparable to the Hubble time in blue down to $\sim 10^6$ yr in purple). The dotted black line denotes the condition $t_{\rm relax} = t_{\rm coll}$, equivalent to $R/R_\odot = [\ln(M/M_\odot)/7.5]^{-1/2}\ M/M_\odot$ for $\eta = 1$, valid regardless of the cluster age and thus coinciding with all intersections of lines with the same color, as can be seen in Figure 3.

The left side of the solid lines in Figure 3 denotes the region where two-body relaxation or collisions can be relevant (i.e., shorter than $t_{\rm H}$) and thus subject to being globally unstable to stellar collisions for $t_{\rm coll}(\leqslant t_H) \leqslant t_{\rm relax}$ and globally stable for $t_{\rm relax} \leqslant t_{\rm coll}$. If the discussed gas dynamical processes are able to populate clusters in the region denoted as "unstable" in green and purple in Figure 3, they will be subject to runaway stellar collisions over the whole system on shorter timescales (in 10^8 and 10^6 yr, respectively), possibly leading to the formation of "naked" MBHs (i.e., without a surrounding cluster) with lower masses than currently observed in NSCs: $M_{\rm BH} \gtrsim 3 \times 10^7\ M_\odot$ for $t_{\rm H} \sim 10^8$ yr (green) and $M_{\rm BH} \gtrsim 3 \times 10^6\ M_\odot$ for $t_{\rm H} \sim 10^6$ yr (purple). In the region below that threshold (intersection of lines with the same color), relaxation processes will operate and the cluster will expand before the onset of runaway collisions is triggered over the whole system, such collisions being restricted to the unstable core, and thus a central MBH is possibly formed that coexists with a surrounding NSC.

Moreover, it is expected at high z to have clusters with a top-heavier IMF, with Population III stars having characteristic masses up to $\sim 100\ M_\odot$, which, in addition to gas dynamical processes, are expected to increase the fraction of collisions by a factor of 10–100, with simulations showing that up to 10% of the (proto)stellar population collides into a single massive object (Boekholt et al. 2018). For that reason, we also analyze the possible role of Population III clusters in Figure 3 by showing in yellow the relaxation and collision timescales for both $\eta = 100$ and $t_{\rm H} = 10^6$ yr. Their intersection increases the mass scale for the formation of "naked" MBHs to $M_{\rm BH} \sim 10^9\ M_\odot$ but reduces by almost 1 order of magnitude the contraction in radius that needs to happen in $\sim 10^6$ yr, opening an interesting possibility for the formation of high-z quasars (Gallerani et al. 2017; Inayoshi et al. 2020) in protogalaxies that are able to fuel this amount of gas ($\sim 10^9\ M_\odot$) to the central ~ 0.1 pc. The dotted red line denotes the condition $t_{\rm relax} = t_{\rm coll}$ for clusters composed of massive $100\ M_\odot$ Population III stars ($\eta = 100$), moving the discussed intersection that denotes the transition between globally stable and unstable regimes up in mass by 2 orders of magnitude, as can be seen by comparing it to the dotted black line in Figure 3. Most likely, the extremely dense, purely gas-free NSC discussed earlier in this paper rarely exists in the early universe, and most often, an unstable NSC will collapse as a whole during its formation before evaporating its gaseous envelope, as might be suggested by the multiple stellar populations seen in the surviving NSCs (Nishiyama & Schodel 2012). On the other hand, if the formation of the surviving NSCs was occurring at high redshift, these would likely be observable with the James Webb Space Telescope (JWST). Since the progenitors of globular clusters are already expected to be detected at high z ($3 \lesssim z \lesssim 8$; Renzini 2017), these most massive progenitors of NSCs should be more likely to be detected, as the number of clusters that could be detected scales linearly with their mass (Renzini 2017).

Certainly, more realistic simulations (with and without gaseous components) are needed to set the open issues, but the absence of NSCs in the collision-dominated regime, with the sharp transition seen at the boundaries of the unstable region of Figure 1, suggests that the fate of the unstable ones is unavoidably collapsing onto an MBH. Therefore, besides all these uncertainties, the results in this work can be taken as supporting evidence that the collapse leading to MBH formation is more likely triggered by runaway collisions than by suppressing fragmentation on smaller scales or, alternatively, by the runaway growth of a preferred IMBH on cosmological timescales. Also, this collision-driven BH formation is a process that could happen even in the earliest epochs of the universe (Korol et al. 2020) without imposing strict constraints on cosmological timescales.

Because it is hard to constrain enough MBH formation through direct observations of such objects by traditional electromagnetic detections, in addition to having more complex and realistic simulations, definite answers will probably come from direct observations of the final collapse by gravitational-wave observatories such as LISA (Amaro-Seoane et al. 2013). In the complex collision-driven collapse scenario described in this paper, it is unlikely that the final collapsing VMS will be close to spherically or axially symmetric; therefore, it is expected to be at least bar-shaped and, most likely, even more irregular, and a gravitational-wave signal is expected from galactic centers at the moment of MBH formation (Rees 1984) that will be detectable in the LISA band out to high redshift (Sun et al. 2017).

I thank Nathan Leigh, Lumen Boco, and Cole Miller for helpful comments. I acknowledge financial support from FONDECYT Regular grant No. 1181663, Millenium Nucleus NCN19_058 (TITANs), and BASAL grant AFB-170002.

References

Amaro-Seoane, P., Aoudia, S., Audley, H., et al. 2013, arXiv:1305.5720
Agarwal, B., Davis, A. J., Khochfar, S., Natarajan, P., & Dunlop, J. S. 2013, MNRAS, 432, 3438
Antonini, F., Capuzzo-Dolcetta, R., Mastrobuono-Battisti, A., & Merritt, D. 2012, ApJ, 750, 111
Antonini, F., Barausse, E., & Silk, J. 2015, ApJ, 812, 72
Arca-Sedda, M., & Capuzzo-Dolcetta, R. 2014, MNRAS, 444, 3738
Arca-Sedda, M., Capuzzo-Dolcetta, R., Antonini, F., & Seth, A. 2015, ApJ, 806, 220
Balcells, M., Graham, A. W., & Peletier, R. F. 2007, ApJ, 665, 1104
Banerjee, S., & Kroupa, P. 2017, A&A, 597, A28
Barause, E., Cardoso, V., & Pani, P. 2015, JPhCS, 610, 012044
Barnes, J. E. 2002, MNRAS, 333, 481
Bate, M. R., Bonnell, I. A., & Broom, V. 2003, MNRAS, 339, 577
Baumgardt, H., Amaro-Seoane, P., & Schodel, R. 2018, A&A, 609, A28
Becerra, F., Greif, T. H., Springel, V., Hernquist, L. E., et al. 2015, MNRAS, 446, 2380
Bellovary, J., Volonteri, M., Governato, F., et al. 2011, ApJ, 742, 13
Binney, J., & Tremaine, S. 2008, Galactic Dynamics (Princeton, NJ: Princeton Univ. Press)
Boco, L., Lapi, A., & Danese, L. 2020, ApJ, 891, 94
Boekholt, T. C. N., Schleicher, D. R. G., Fellhauer, M., et al. 2018, MNRAS, 476, 366
Böker, T., Sarzi, M., McLaughlin, D. E., et al. 2004, AJ, 127, 105
Bromm, V., & Loeb, A. 2003, ApJ, 596, 34
Cappellari, M., Bacon, R., Bureau, M., et al. 2006, MNRAS, 366, 1126
Capuzzo-Dolcetta, R. 1993, ApJ, 415, 616
Côté, P., Piatek, S., Ferrarese, L., et al. 2006, ApJS, 165, 57
Davies, M. B., Miller, M. C., & Bellovary, J. M. 2011, ApJL, 740, L42
Devecchi, B., & Volonteri, M. 2009, ApJL, 694, 302
Devecchi, B., Volonteri, M., Rossi, E. M., Colpi, M., & Portegies Zwart, S. 2012, MNRAS, 421, 1465
Dubois, Y., Volonteri, M., Silk, J., et al. 2015, MNRAS, 452, 1502
Elmegreen, B. G., Bournaud, F., & Elmegreen, D. M. 2008, ApJ, 684, 829
Escala, A. 2006, ApJL, 648, L13
Escala, A. 2007, ApJ, 671, 1264
Escala, A. 2011, ApJ, 735, 56
Escala, A., & Larson, R. B. 2008, ApJL, 685, L31
Ferrarese, F., & Merritt, D. 2000, ApJL, 539, L9
Ferrarese, L., Côté, P., Dalla, B., et al. 2006, ApJL, 644, L21
Freitag, M., Gurkan, M. A., & Rasio, F. A. 2006a, MNRAS, 368, 141
Freitag, M., Rasio, F. A., & Baumgardt, H. 2006b, MNRAS, 368, 121
Gebhardt, K., Bender, R., Bower, G., et al. 2000, ApJL, 539, L13
Georgiev, I. Y., Böker, T., Leigh, N., Lützgendorf, N., & Neumayer, N. 2016, MNRAS, 457, 2122
Ghez, A. M., Salim, S., Weinberg, N. N., et al. 2008, ApJ, 689, 1044
Gieles, M., Moeckel, N., & Clarke, C. J. 2012, MNRAS, 426, L11
Gillessen, S., Eisenhauer, F., Fritz, T. K., et al. 2009, ApJL, 707, L114
Gnedin, O. Y. 2001, CQGra, 18, 3983
Goswami, S., Umbreit, S., Bierbaum, M., & Rasio, F. A. 2012, ApJ, 752, 43
Graham, A. W. 2012, MNRAS, 422, 1586
Gultekin, K., Richstone, D. O., Gebhardt, K., et al. 2009, ApJ, 698, 198
Gurkan, M. A., Freitag, M., & Rasio, F. A. 2004, ApJ, 604, 632
Henon, M. 1965, AnAp, 28, 62
Hopkins, P. F., & Quataert, E. 2010, MNRAS, 407, 1529
Inayoshi, K., & Haiman, Z. 2014, MNRAS, 445, 1549
Inayoshi, K., Visbal, E., & Haimman, Z. 2020, ARA&A, 58, 27
Jeans, J. H. 1902, RSPTA, 199, 1
Korol, V., Mandel, I., Miller, M. C., et al. 2020, MNRAS, 496, 994
Landau, L. D., & Lifshitz, E. M. 1980, Course of theoretical physics (Oxford: Pergamon Press)
Latif, M. A., & Schleicher, D. R. G. 2015, A&A, 578, A118
Lee, H. M. 1987, ApJ, 319, 801
Leigh, N., Böker, T., & Knigge, C. 2012, MNRAS, 424, 2130
Leigh, N. W. C., Lützgendorf, N., Geller, A. M., et al. 2014, MNRAS, 444, 29
Leigh, N., Georgiev, I. Y., Böker, T., Knigge, C., & den Brok, M. 2015, MNRAS, 451, 859
Lodato, G., & Natarajan, P. 2006, MNRAS, 371, 1813L
Lupi, A., Colpi, M., Devecchi, B., Galanti, G., Volonteri, M., et al. 2014, MNRAS, 442, 3616
Madau, P., & Rees, M. J. 2001, ApJL, 551, L27
Magorrian, J., Tremaine, S., Richstone, D., et al. 1998, ApJ, 115, 2285
Mayer, L., Kazantzidis, S., Escala, A., & Callegari, S 2010, Natur, 466, 1082
Miller, M. C., & Davies, M. B. 2012, ApJ, 755, 81
Neumayer, N., Seth, A., & Böker, T. 2020, A&ARv, 28, 4
Nishiyama, S., & Schodel, R. 2012, A&A, 549, A57
Omukai, K., Schneider, R., & Haiman, Z. 2008, ApJ, 686, 801
Oppenheimer, J. R., & Volkoff, G. M. 1939, PhRv, 55, 374
Padoan, P., Juvela, M., Pan, L., Haugbølle, T., & Nordlund, Å 2016, ApJ, 826, 140
Pamanarev, T., Just, A., Spurzem, R., et al. 2019, MNRAS, 484, 3279
Portegies Zwart, S. F., & McMillan, S. L. W. 2002, ApJ, 576, 899
Portegies Zwart, S. F., Makino, J., McMillan, S. L. W., & Hut, P. 1999, A&A, 348, 117
Prieto, J., Escala, A., Privon, G., & d'Etigny, J. 2020, arXiv:2101.09407
Prieto, J., & Escala, A. 2016, MNRAS, 460, 4018
Prieto, J., Escala, A., Volonteri, M., & Dubois, Y. 2017, ApJ, 836, 216
Quinlan, G. D., & Shapiro, S. L. 1990, ApJ, 356, 483
Rees, M. J. 1984, ARA&A, 22, 471
Rees, M. J., & Ostriker, J. P. 1977, MNRAS, 179, 541
Regan, J. A., & Downes, T. P. 2018, MNRAS, 475, 4636
Regan, M. W., & Teuben, P. J. 2004, ApJ, 600, 595
Reinoso, B., Schleicher, D. R. G., Fellhauer, M., Klessen, R. S., & Boekholt, T. C. N. 2018, A&A, 614, A14
Renzini, A. 2017, MNRAS Letters, 469, L67
Ricarte, A., & Natarajan, P. 2018, MNRAS, 481, 3278
Sakurai, Y., Yoshida, N., Fujii, M. S., & Hirano, S. 2018, ApJ, 855, 17
Salpeter, E. 1964, ApJ, 140, 796
Sanders, R. H. 1970, ApJ, 162, 791
Sarazin, C. L., & White, R. E. 1987, ApJ, 320, 32
Schleicher, D. R. G., Palla, F., Ferrara, A., Galli, D., & Latif, M. 2013, A&A, 558, A59
Shang, C., Bryan, G. L., & Haiman, Z. 2010, MNRAS, 402, 1249
Shapiro, S. L. 2004, Carnegie Observatories Astrophysics Series, Vol. 1: Coevolution of Black Holes and Galaxies (Cambridge: Cambridge Univ. Press), 103
Shapiro, S. L., & Teukolsky, S. A. 1985, ApJ, 292, L41
Shlosman, I., Begelman, M. C., & Frank, J. 1990, Natur, 345, 679
Shu, F. H. 1991, The Physics of Astrophysics, Vol. 2 (Mill Valley, CA: Univ. Science Books)
Spergel, D. N., Verde, L., Peiris, H. V., et al. 2003, ApJS, 148, 175
Spitzer, L. J. 1969, ApJ, 158, L139
Stone, N. C., Kupper, A. H. W., & Ostriker, J. P. 2017, MNRAS, 467, 4180
Suazo, M., Prieto, J., Escala, A., & Schleicher, D. R. G. 2019, ApJ, 885, 127
Sun, L., Paschalidis, V., Ruiz, M., & Shapiro, S. L. 2017, PhRvD, 96, 043006
The Event Horizon Telescope Collaboration 2019, ApJL, 875, L1
Tolman, R. C. 1934, PNAS, 20, 169
Toomre, A. 1964, ApJ, 139, 1217
Tremaine, S. D. 1976, ApJ, 203, 345
Vishniac, E. T. 1978, ApJ, 223, 986
Volonteri, M., & Begelman, M. C. 2010, MNRAS, 409, 1022
Volonteri, M. 2010, A&ARv, 18, 279
Volonteri, M., & Rees, M. J. 2006, ApJ, 650, 669
Volonteri, M., Haardt, F., & Madau, P. 2003, ApJ, 582, 559
Walcher, C. J., Böker, T., Charlot, S., et al. 2006, ApJ, 649, 692
Zel'dovich, Ya 1964, SPhD, 9, 195
Zel'dovich, Ya. B., & Podurets, M. A. 1965, AZh, 42, 963